PATTERN SIZE IN GAUSSIAN FIELDS FROM SPINODAL DECOMPOSITION

LUIGI AMEDEO BIANCHI, DIRK BLÖMKER, AND PHILIPP WACKER

Abstract. We study the two-dimensional snake-like pattern that arises in phase separation of alloys described by spinodal decomposition in the Cahn-Hilliard model. These are somewhat universal patterns due to an overlay of eigenfunctions of the Laplacian with a similar wave-number. Similar structures appear in other models like reaction-diffusion systems describing animal coats' patterns or vegetation patterns in desertification.

Our main result studies random functions given by cosine Fourier series with independent Gaussian coefficients, that dominate the dynamics in the Cahn-Hilliard model. This is not a cosine process, as the sum is taken over domains in Fourier space that not only grow and scale with a parameter of order $1/\varepsilon$, but also move to infinity. Moreover, the model under consideration is neither stationary nor isotropic.

To study the pattern size of nodal domains we consider the density of zeros on any straight line through the spatial domain. Using a theorem by Edelman and Kostlan and weighted ergodic theorems that ensure the convergence of the moving sums, we show that the average distance of zeros is asymptotically of order ε with a precisely given constant.

1. Introduction

We are interested in studying the patterns that form in the solution of the stochastic Cahn-Hilliard equation during the separation process called spinodal decomposition. This equation, originally introduced in [10] and [11], models the relative concentration of two components in an alloy after quenching an initially homogeneous mixture.

Similar structures appear in many other situations. One example are the patterns in coats of animals like zebras or tigers [31], where the underlying system is a reaction-diffusion system with a Turing instability, as argued by Sander and Wanner in [36]. Another occurrence are the vegetation patterns in desertification like the one observed for the tiger bush in Africa, as studied for example by Siero, Siteur et al. in [37, 38]. In those papers they provide a mathematical study of the emergence of pattern on an unbounded domain in the extended Klausmeier model, which is similar to a reaction-diffusion system.

More similar to the Cahn-Hilliard setting is the Swift-Hohenberg equation (see for example the review [14]). A result very much related to the result presented here is given by Blömker and Maier-Paape in [5]. The main difference is that significantly fewer Fourier-modes determine the pattern. The initial stage of hill formation of an example from surface growth [25, 32] also used in ion sputtering [30] exhibits similar patterns, too. For details see the review article [9].

We believe that in all these examples the characteristic snake like pattern that appear initially is mainly due to random composition of eigenfunctions of the Laplacian of similar wave-length, where

Date: November 18, 2015.

2010 *Mathematics Subject Classification.* **60H15**, 60H05, 60G15, 60G60.

Key words and phrases. Cahn-Hillard equation, pattern size, Gaussian fields, ergodic theorem.

P.W. was supported by a Cusanuswerk scholarship. L.A.B. was supported by the German Science Foundation (DFG), grant number BL 535/9-2 "Mehrskalenanalyse stochastischer partieller Differentialgleichungen (SPDEs)".

the solution is described by a high dimensional strongly unstable space and the nonlinearity does not yet play a significant role. In order to outline this idea, we focus in the following sections on the stochastic Cahn-Hilliard equation on the square.

The main question that we want to answer rigorously in this paper is the following:

What is the characteristic thickness of the pattern (i.e. the snake-like structures)?

To address this, we count the (average) number of zeros on any straight line across the domain, using a result given by Edelman and Kostlan in [19].

In the context of spinodal decomposition, a partial result was obtained by Maier-Paape and Wanner in [28], where they tried to estimate the size of balls that would fit into the nodal domain. A numerical computation of Betti numbers was performed in a series of papers [16, 17, 20].

Moreover the structure of nodal domains for Gaussian random fields is the topic of numerous recent publications, which we do not try to survey in full detail. Under the assumption of stationarity and isotropy there are asymptotic results on the numer of zeros along lines. See for example [18,27]. Minkowski-functionals are also treated (see [2] for a review), or [39] for references to asymptotic results of the number of connected components. We comment on these approaches later on in more detail.

1.1. **The Cahn-Hilliard-Cook equation.** The stochastic Cahn-Hilliard (or Cahn-Hilliard-Cook) equation was introduced by Cook in [12] as a stochastic modification of the originally deterministic model. It can be written as follows:

$$\partial_t u = -\Delta(\varepsilon^2 \Delta u + f(u)) + \partial_t W,$$

where the noise $\partial_t W$ is the derivative of a Q-Wiener process and f is the derivative of a double well potential, where a standard choice is $f(u) = u - u^3$, although the true nonlinearity introduced by Cahn and Hilliard should exhibit logarithmic poles. We consider it on the square domain $[0,1]^2$, with Neumann boundary conditions $\partial_\nu u = \partial_n u \Delta u$. In the physical model of alloys, u models the rescaled concentration of one component, and the extreme values $u = \pm 1$ correspond to 0% and 100% concentration of the first component in any point.

The canonical initial condition for the phase separation in spinodal decomposition is a homogeneous concentration, constant on the whole domain. Due to the presence of the noise, after some time the homogeneous picture is broken, decomposition starts playing its role and snake-like pattern appear and persist, giving place to situations like the one simulated in Figure 1.

For the Cahn-Hilliard equation, one can consider the set of the most unstable eigenvalues, which dominate the dynamics for a long time, also called "strongly unstable subspace". This was studied in the deterministic model by Maier-Paape and Wanner in [28,29] and later in the stochastic setting by Blömker, Maier-Paape and Wanner in [6, 8] (see also the review [7]). Later Sander and Wanner extended in [35] the approximation result by linearisation to unexpectedly large radii.

It is interesting to notice that the evolution of pattern complexity in the spinodal decomposition seems to be quite different in the deterministic model with random initial conditions or the stochastic model with constant initial condition. In [20] it was shown numerically that the deterministic model exhibits an unnatural increase of complexity during the separation process.

1.2. **Linearised Cahn-Hilliard-Cook equation.** While the Cahn-Hilliard equation is highly nonlinear, its dynamics is reasonably well approximated by linearisation in the first phase up to unexpectedly large radii. So let us discuss the linearised system (around the initial conditions $u = m$) to motivate why we study random cosine series later.

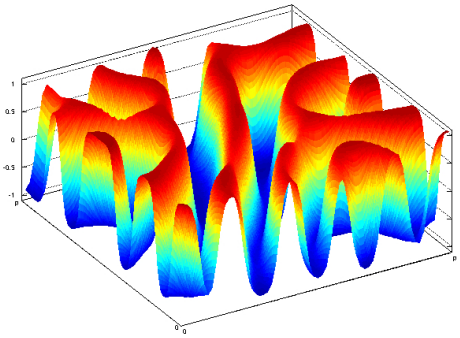

FIGURE 1. Pattern in Spinodal decomposition. The snake-like pattern appears as the nodal domains in the level set of the average concentration 0.

Such linearised system can be written as

$$\partial_t u = Au + \partial_t W\,, \qquad u(0) = m, \tag{1}$$

where $A = -\varepsilon^2\Delta^2 - \Delta f'(m)$ is a self-adjoint linear operator having a complete orthonormal system of eigenfunctions. In our study we focus on the simple domain $[0,1]^2$ to avoid additional pattern complexity introduced by a complicated shape of the boundary. The L^2-basis on the square is made of cosine functions

$$e_{k,l}(x) = C\cos(k\pi x)\cos(l\pi y),$$

with $Ae_{k,l} = \lambda_{k,l}e_{k,l}$, where

$$\lambda_{k,l} = -\varepsilon^2(k^2+l^2)^2\pi^4 + (k^2+l^2)\pi^2 f'(m).$$

The solution to (1) is given by the stochastic convolution (see [15]), which simplifies here to a cosine series with random coefficients.

$$W_A(t) = \sum_{k,l\in\mathbb{N}} \int_0^t e^{(t-s)A}\,\mathrm{d}W(s) = \sum_{k,l\in\mathbb{N}} \alpha_{k,l}\int_0^t e^{(t-s)\lambda_{k,l}}\,\mathrm{d}B_{k,l}(s)e_{k,l},$$

where the B_k are independent Brownian motions and the Q-Wiener process W has a joint eigenbasis with A such that $Qe_{k,l} = \alpha_{k,l}^2 e_{k,l}$. This is a usual but quite strong assumption, that Q commutes with A. As this is only our motivating example, for simplicity of presentation we do not enter this discussion here. Some details and further references can be found in [7]. One also could think of space-time white noise, where Q is the identity and thus all α_k are one.

The strongly unstable subspace also called "strong subspace", for short, is defined in Fourier space by the wave-vectors

$$R_\varepsilon^\gamma := \{(k,l)\in\mathbb{N}^2 : \lambda_{k,l} > \gamma\lambda_{\max}\},$$

for some $\gamma\in(0,1)$ close to 1. In particular, in the two-dimensional setting we consider, the set R_ε^γ is a quarter-ring in the $\mathbb{N}^2$ lattice, containing $\mathcal{O}(\varepsilon^{-2})$ many wave-vectors corresponding to eigenvalues close to the maximum. In the following we do not always specify the explicit dependence of R_ε^γ on γ and write R_ε for short. Note that this set not only is growing in size for $\varepsilon\to 0$, but also moves as a whole towards infinity.

As already outlined, as long as the solution is not too large, the dynamics of the nonlinear Cahn-Hilliard equation is dominated by the projection P_{R_ε} of the stochastic convolution on the strong

subspace. By this we mean the restriction of the Fourier series to wave-vectors in R_ε, which is given by

$$P_{R_\varepsilon} W_A(t) = \sum_{m=(k,l)\in R_\varepsilon} \alpha_m c_m e_m, \qquad \text{with} \quad c_m = \int_0^t e^{(t-s)\lambda_m} \, \mathrm{d}B_m(s) \, .$$

The random variables in the family $\{c_m\}_{m\in R_\varepsilon}$ are by definition independent centred Gaussians. By Itō-isometry the variance of c_m is

$$\mathbb{E}c_m^2 = \int_0^t e^{(t-s)2\lambda_m} \, \mathrm{d}s = \frac{1}{2\lambda_m}(1 - e^{-2\lambda_m t}) \approx \frac{1}{2\lambda_m} = \mathcal{O}(\varepsilon^2),$$

for times $t \approx \varepsilon^2$, which is close to the time-scale on which the first phase of spinodal decomposition was described (see [6]), recalling that $\lambda_m = \mathcal{O}(\varepsilon^{-2})$, as it is of order of the largest eigenvalue. Hence after linearisation and projection via P_{R_ε}, the solution at a fixed time t seems to be well approximated by

$$u(x,y) \approx \sum_{(k,l)\in R_\varepsilon} c_{k,l} \cdot \cos(k\pi x)\cos(l\pi y), \tag{2}$$

where the $c_{k,l}$ are independent centred Gaussians with similar variances. This motivates the choice of our toy model, which we will present in the next subsection, fixing for ease of presentation all the variances of the coefficients to be the same.

1.3. **Random Fourier Series.** For the main part of the paper we consider the random function

$$f(x,y) = \sum_{(k,l)\in R_\varepsilon} c_{k,l} \cdot \cos(k\pi x)\cos(l\pi y), \tag{3}$$

on the unit square $x, y \in [0,1]^2$, with the random coefficients $c_{k,l}$ being independent and identically distributed centred Gaussian random variables. Later we discuss also the impact of other domains in Fourier space, and not only the ring.

As we showed in the previous subsection, this is a simplified version (adding the identically distributed assumption) of the approximation (2) of the stochastic Cahn-Hilliard equation. We furthermore set the variance to be 1, i.e. $c_{k,l} \sim N(0,1)$. Doing this, we ignore both the time-dependence and the inhomogeneity in the growth rates of the strong Fourier modes for the sake of simplicity.

We define the subset R_ε of strong modes, introduced above in the Cahn-Hilliard case, as

$$R_\varepsilon = \{(k,l) \in \mathbb{N}^2 |\ \alpha_\ominus < \sqrt{(k\varepsilon)^2 + (l\varepsilon)^2} < \alpha_\oplus\},$$

where the parameters are

$$\alpha_\oplus = \sqrt{\frac{1+\sqrt{1-\gamma}}{2\pi^2}} \quad \text{and} \quad \alpha_\ominus = \sqrt{\frac{1-\sqrt{1-\gamma}}{2\pi^2}} \quad \text{with} \quad \gamma \in (0,1).$$

Although the model (3) is somewhat reminiscent of the cosine-process (see e.g. [1]) or the random wave model (see e.g. [18]), it is fundamentally different in the sense that it is neither stationary nor isotropic. The law of the random function f might change under translation or rotation (as a function extended to $\mathbb{R}^2$). It is an easy calculation to show that $f(x)$ is a centered Gaussian with covariance

$$\mathbb{E}f(x)f(y) = q(x+y) + q(x-y) \quad \text{for} \quad q(z) = \frac{1}{2} \sum_{(k,l)\in R_\varepsilon} \cos(k\pi z)\cos(l\pi z) \, .$$

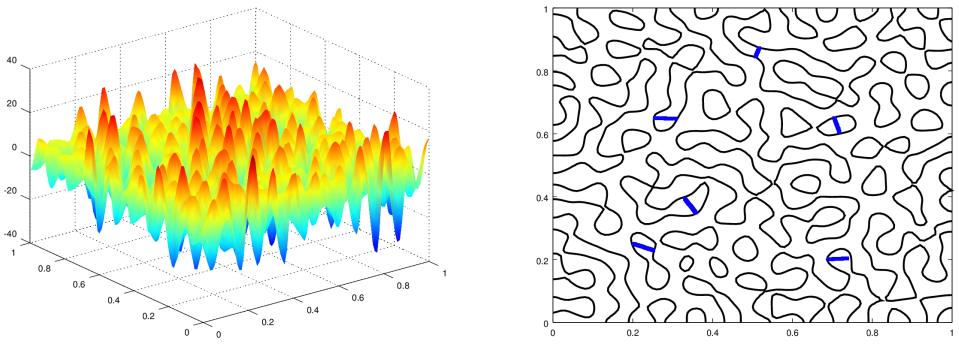

FIGURE 2. A simulation of the function f for $\gamma = 0.8$ with a plot of its zero-level set. On the latter we picked some measurements of the pattern thickness. Empirically, the average distance is $2\pi\varepsilon$. There is of course some variation and there are areas and directions where the thickness is much higher or lower.

1.4. **Pattern size.** A simulation of (3) is presented in Figure 2. We can see the snake-like patterns which are characteristic of the Cahn-Hilliard model. It appears from the numerical simulations that the thickness of the structures is somewhat proportional to ε, as it is shown in Figure 2. Here we propose to measure such thickness as the distance between consecutive zeros of the solution considered on an arbitrary line through the domain, as exhibited in Figure 3.

This definition of a pattern size is intuitively the right one, as the dominating Fourier space R_ε consists of frequencies given by the wave-vector $(k,l) \in R_\varepsilon$ are all of the order of magnitude of the wave-number $|(k,l)|$ which is ε^{-1}, and hence the average distance is conjectured to be of the same order as $C'\varepsilon$. Although this line of reasoning sounds very plausible, in the wave-vector the individual frequencies can vary vastly. Moreover we will also see later in the main results, that when counting zeros on arbitrary straight lines, only the scaling of the upper bound for the wave number seems to be essential. Let us remark that for stationary isotropic Gaussian fields there are quite a few publications on the average density of zeros along lines. They already date back to the work of Rice [33] or Longuet-Higgins [27], [26]. See also Dennis [18]. Their approach yields qualitatively similar results of a pattern size of order ε for models given by cosine series similar to (3), but none of those methods seem to apply straightforwardly to (3), in that they usually assume isotropy and stationarity.

A rigorous quantification of the geometry and topology of Cahn-Hilliard-Cook patterns is still an open problem, though. The first attempt in the setting of spinodal decomposition by Maier-Paape and Wanner in [28] yielded a partial result by bounding the radii of balls that would fit into the nodal domain. That strategy worked completely only in the setting of [5], where the ring R_ε was still growing, but its size was smaller by a small power in ε.

As already mentioned in the previous subsection, recent numerical work on the number of components in the pattern has been done, using rigorous methods from computational algebraic topology to compute the Betti numbers, by Gameiro, Mischaikow and Wanner in [20] or similarly by Day, Kalies, Mischaikow and Wanner in [16,17]. See also Guo and Hwang [23] and Sander and Tatum [34] for additional results on the pattern in Cahn-Hilliard equation. Let us recall that Betti numbers

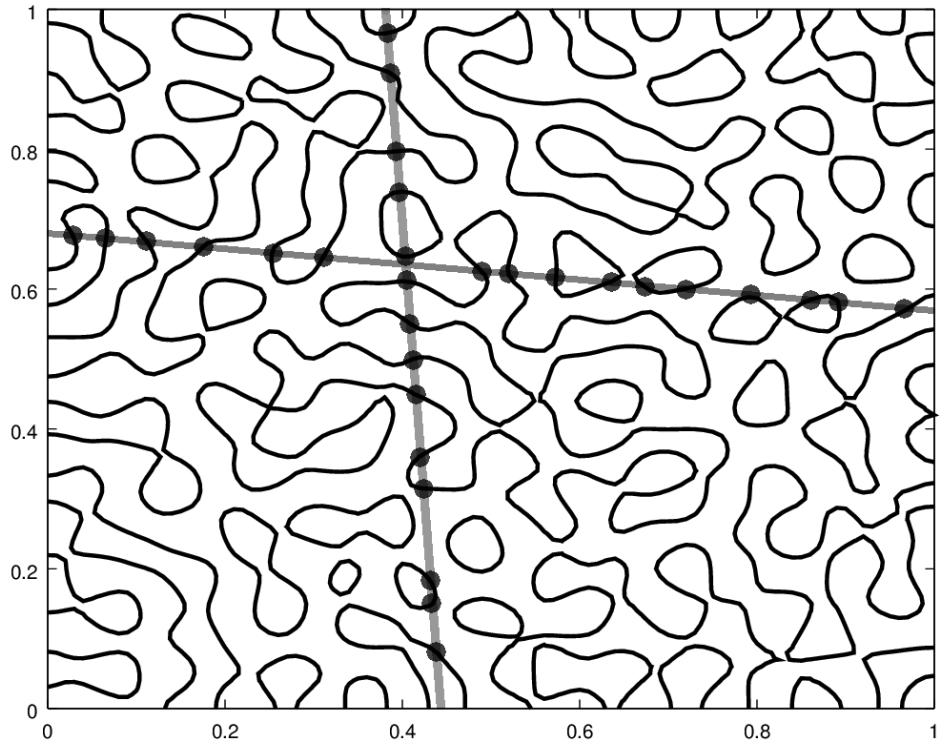

FIGURE 3. Pattern size computation of the function f by inserting arbitrary lines through the spatial domain $[0,1]^2$, where we represent the zero level sets for our model in the Fourier domain $R_{0.01}$. The zeros are order ε apart, on average.

for the two-dimensional nodal domain count the number of connected components and the number of holes.

For general stationary or isotropic Gaussian fields there is also some work on Minkowski functionals measuring the area and the number of connected components of the nodal domain as well as the length of the set of level 0. See [2], for a collection of results. But even the precise constant in the asymptotic behaviour of the number of connected components seems to be still an open problem. See [39] for further references. None of these results seems to fit to (3) anyway, not just because of the assumptions on isotropy and stationarity, but also because we are summing over index sets that are not only growing, but also moving, and thus the asymptotic limit is not clear.

2. Main result

The question we aim to rigorously answer is:

Question 1. *What is the characteristic thickness of the pattern (i.e. snake-like structures) in our model $f(x,y)$ defined in* (3)*, on the unit square $(x,y) \in [0,1]^2$?*

In Figure 2 we can see that the average thickness appears to be $2\pi\varepsilon$, which we will prove to be the case.

To address Question 1, we take the following approach: we draw a straight line across the unit square and we count the (average) number of zeros of f on that segment, see Figure 3. Then we divide the length of the segment by the number of zeros, obtaining the average distance between zeros, that is the average pattern size. So the problem reduces to counting the number of zeros of f, a random function, and a way of doing this is provided (in a more general form than reported here) by Edelman and Kostlan in [19]:

Theorem 1 (Number of real zeros of a random function)**.** *Let $v(x) = (f_0(x), \dots, f_n(x))^T$ be any collection of differentiable functions and $c_0, \dots, c_n$ be independent and identically distributed Gaussians centred in 0. Given the function*

$$h(x) = \sum_{k=0}^{n} c_k \cdot f_k(x),$$

the density of real zeros of h on an interval I is

$$\delta(x) = \frac{1}{\pi} \left\| \frac{\mathrm{d}}{\mathrm{d}x} w(x) \right\|_{\mathbb{R}^n}, \qquad \text{where} \qquad w(x) = \frac{v(x)}{\|v(x)\|_{\mathbb{R}^n}}.$$

The expected number of real zeros of h on I is then

$$\int_I \delta(x)\, \mathrm{d}x.$$

Theorem 1 holds for functions h on the real line, so we need to translate our two-dimensional problem f to an equivalent one formulated on a line. In the following first we consider f constrained on an arbitrary *horizontal* line at height t, which is

$$L_t = \{(x, t) : x \in [0, 1]\} \quad \text{for} \quad t \in [0, 1]\,.$$

We obtain a function of one variable and can apply Theorem 1. The generalization to arbitrary (non-horizontal) lines as the ones depicted in Figure 3 is a straightforward generalization and is discussed in Section 6 but the underlying idea does not change.

We need to introduce, in the spirit of Theorem 1, the following notation:

$$w_t(x) = \left(\frac{\cos(k\pi x)\cos(l\pi t)}{\sqrt{\sum_{m,n \in R_\varepsilon} \cos^2(m\pi x)\cos^2(n\pi t)}} \right)_{(k,l)\in R_\varepsilon}$$

$$W_t(x) = \left\| \left(\frac{\mathrm{d}}{\mathrm{d}x} w_t(x) \right)_{(k,l)\in R_\varepsilon} \right\|^2 = \frac{S_3}{S_1} - \left(\frac{S_2}{S_1} \right)^2,$$

where we have

$$S_1 = \sum_{m,n \in R_\varepsilon} \cos^2(m\pi x)\cos^2(n\pi t)$$

$$S_2 = \sum_{m,n \in R_\varepsilon} m\pi \cos(m\pi x)\sin(m\pi x)\cos^2(n\pi t)$$

$$S_3 = \sum_{m,n \in R_\varepsilon} m^2\pi^2 \sin^2(m\pi x)\cos^2(n\pi t).$$

Theorem 2. *For any $\gamma \in (0,1)$ and any horizontal line L_t for $x,t \in (0,1)$ the function $W_t(x)$ defined on L_t behaves asymptotically as $(2\varepsilon)^{-2}$ for $\varepsilon \to 0$.*

This means in particular that the average number of zeros is $(2\pi\varepsilon)^{-1}$, so the mean pattern size (i.e. the average distance from any zero on any line to the next zero) is $2\pi\varepsilon$.

Remark 3. *It is a remarkable fact that the result of Theorem 2 is independent of γ, because the number of Fourier modes involved is much smaller for $\gamma \approx 1$ than for $\gamma \approx 0$. As we can see in Figure 4, while the average asymptotic pattern size along lines remains the same, the domain with higher γ looks more organized. The pattern seems to be "more regular" in some sense that our method cannot detect.*

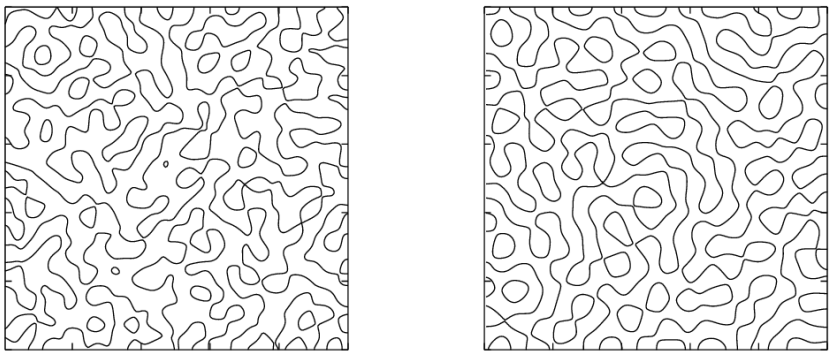

FIGURE 4. Patterns generated in the Fourier domains $R^{0.1}_{0.01}$ (left) and $R^{0.9}_{0.01}$ (right)

For the proof of Theorem 2 we have to show that

$$\lim_{\varepsilon\to 0} \varepsilon \frac{S_2}{S_1} = 0 \qquad\qquad \lim_{\varepsilon\to 0} \varepsilon^2 \frac{S_3}{S_1} = \frac{1}{4},$$

which we do in Lemma 12. The main idea behind the proof is that the sums S_i, $i = 1,2,3$ can be calculated in the limit via ergodic-type theorems.

Remark 4. *From here onwards we fix $x,t \in (0,1)$, as the functions behave a little differently on the borders. If we have $t = 0,1$, we lose all the terms in t, that become identically 1, but we obtain anyway the same result. The cases $x = 0,1$ are not interesting, as the* sin *is always zero and thus $W_t(0) = W_t(1) = 0$. But since we are looking for a density in terms of x, considering it in a single point does not provide any useful information.*

We will prove the main result in Section 3. After that in Section 4 we state the generalization of the main result to general domains in Fourier space different from the quarter-ring and give a few explicit examples that the main result is still true, although the patterns appearing might look quite different.

As our result is a purely asymptotic one, we give a few examples in Section 4, where the number of zeros agrees very well with the asymptotic prediction even for moderate ε. In Section 5, we calculate numerically the functions $\delta(x)$ or $W_t(x)$ for different values of ε. There (cf. also Figure 8) we see already for moderate ε a fast and uniform convergence apart from any small layer at the boundary.

Finally in Section 6 we briefly discuss the case of sloped lines, which is a straightforward generalization, up to some additional technicalities. In the Appendix we show that we can establish convergence in the rational case not treated in the proof, where we cannot use Birkhoff's ergodic theorem.

Let us comment on further generalizations that are within the scope of this approach. First we can easily incorporate the case where the Gaussians are not all identically distributed. For instance when the noise is diagonal w.r.t. the cosine modes, we just obtain additional weights in the main result, coming from the eigenvalues of the covariance operator of the noise.

For different domains in Fourier space we always get the same order of zeros on any line through the domain, but as we can see in Figure 7 the pattern might look quite different. Further characterizations using Betti numbers as in [20], the Minkowski-functionals as in [2] or bounds on the radii of balls in the nodal domains as in [28] might help to understand why the pattern in spinodal decomposition is so special, as it appears to be quite regular, but not too symmetric.

Moreover, we believe that the result on the square $[0,1]^2$ is not that special, and with the same method we should be able to treat three or higher dimensional problems. We have to stress that there are technical problems extending the result to general domains, especially when the boundary has a complicated geometry. In the proof for arbitrary domains we only need to replace the cosines by the corresponding eigenfunctions. We should then use the ergodic theorem to recover the convergence of the sums, but there is no guarantee that we can still do that, the main technical problem being that we cannot easily isolate the wavenumber as an argument of the function. Moreover, even if we could, the reduction of the two-dimensional Birkhoff ergodic theorem to the one dimensional case is not always possible: we would need to prove a true two-dimensional ergodic theorem, but such results are available in the literature.

3. Proof of the main result

The main result is on one hand based on an application of the theorem by Edelman and Kostlan. On the other hand, for the asymptotic behaviour we need the convergence of series over growing domains and the value of the limit. This is established by a two-dimensional weighted Birkhoff ergodic theorem. There is a vast literature on ergodic theorems, and the theory is far developed, so we do not attempt to give an overview. We just refer to [21, 22] for ergodic theorems on abstract groups or subgroups of lattices.

In the following we first state the one dimensional ergodic theorem, then give a direct prove for a weighted ergodic theorem on arbitrary domains based on the analogous result on squares (see for example [24]). We also give an elementary proof that the usual ergodic theorem implies (under some conditions on the weights) a weighted version. Let us remark that the results we need are not in the usual setting of weighted ergodic theorems, as for example in the theory of "good weights" (see for example [3, 4]), because we allow the weights to grow and furthermore we change the normalising constant in front of the sum.

3.1. Ergodic theorem.

Given a σ-algebra, a transformation T is said to be *uniquely ergodic* if it has a unique ergodic measure. The map $z \mapsto z + \alpha$ on the unit circle is uniquely ergodic if and only if α is irrational. In this case the unique ergodic measure is the Lebesgue measure.

Theorem 5 (Birkhoff ergodic theorem, see [13])**.** *Let (X, μ) be a probability space. If T is μ-invariant and ergodic and g is integrable, then for a.e. $z \in X$*

$$\lim_{N\to\infty} \frac{1}{N} \sum_{k=1}^{N} g\left(T^k(z)\right) = \int_X g(\zeta)\,\mathrm{d}\mu(\zeta). \tag{4}$$

Moreover if T is continuous and uniquely ergodic with measure μ and if g is continuous, then (4) *holds for all $z \in X$ (instead of a.e.).*

Remark 6. *Having the result to hold for all initial conditions is of paramount importance, as we require it to hold for some specific initial values. We will then look for uniquely ergodic transformations.*

Remark 7. *If X has dimension 2, Theorem 5 can be stated in the following form. See for example Theorem 1.9 of [21] for an abstract version of this theorem on groups.*

$$\lim_{N\to\infty} \frac{1}{N^2} \sum_{k,l\in\{1,\dots,N\}^2} (g \circ T^{(k,l)})(y, v) = \iint_X g\,\mathrm{d}\mu$$

Nevertheless, we do not need an abstract proof of a two-dimensional ergodic theorem, as all our functions factor, so we can always reduce the ergodic theorem on the square directly to the one-dimensional case.

3.2. **The weighted averaging condition.** First we draft a necessary requirement for averaged weighted sums fulfilling an ergodic-type property on a rectangle-shaped summation domain. Then we show that this can be used to obtain summation on more general domains. In our case this is a quarter-ring-shaped subset in $\mathbb{N}^2$.

After that we show that the sums we need to calculate all fulfil this requirement.

Requirement (Weighted averaging condition)**.** *Let $([0,1]^d, \lambda)$ be the probability space with the Lebesgue-measure λ. We say that $(f, (a_m))$ with $f : [0,1]^d \to \mathbb{R}$ continuous and extended by periodicity to $\mathbb{R}^d$ and $a_m \in \mathbb{R}$ fulfils the weighted averaging condition, if for every $x^0 \in [0,1]^d$, every $\alpha \in \mathbb{N}^d$ and*

$$Q_L = \bigotimes_{i=1}^{d} [1, \dots, \alpha_i L] \cap \mathbb{N}^d,$$

the following assumption holds:

$$\frac{1}{\sum_{m\in Q_L} a_m} \sum_{m\in Q_L} a_m \cdot f(m_1 x_1^0, m_2 x_2^0, \dots, m_d x_d^0) \xrightarrow{L\to\infty} \int_{[0,1]^d} f(x)\,\mathrm{d}x\,.$$

For any open set $M \subset \mathbb{R}^d_+$ we define

$$M_L = (L \cdot M) \cap \mathbb{N}^d,$$

the projection on the positive integers of its scaled version. We define

$$|M_L|_a = \sum_{m\in M_L} a_m$$

and denote by $|M_L|$ the cardinality of M_L.

Requirement (Generation of measures)**.** *We require that the weights $a = (a_m)$ generate a measure λ_a on $\mathbb{R}^d_+$ which is equivalent to the Lebesgue measure λ, i.e. there exists an $\alpha > 0$ such that for each set with open interior $M \subset \mathbb{R}^d_+$,*

$$L^{-\alpha}|M_L|_a \xrightarrow{L\to\infty} \lambda_a(M).$$

Let us remark that in general, we could get the result for a weaker assumption on the measure λ_a than being equivalent to Lebesgue measure. But as in all our examples this is the case, we assume this for simplicity of presentation.

The trivial example for the generation of measures are the constant weights $a_{k,l} = 1$ that generate the Lebesgue measure with $\alpha = d$.

Example 8. *An example that is used frequently later is $a_{k,l} = k^2$ for dimension $d = 2$. Then by Riemann sum approximation*

$$L^{-4}|M_L|_a = L^{-4} \sum_{(k,l)\in L\cdot M} k^2 = \sum_{(k,l)\in M\cap \frac{1}{L}\mathbb{N}^2} k^2 L^{-2} \xrightarrow{L\to\infty} \int_M \xi^2 \,\mathrm{d}(\xi,\eta)\ .$$

Thus the measure $\lambda_{(k^2,1)}$ generated by the weight has a Lebesgue-density $(\xi,\eta) \mapsto \xi^2$. As the density is up to the Lebesgue null set $\xi = 0$ everywhere strictly positive, the measures $\lambda_{(k^2,1)}$ and λ are equivalent.

Lemma 9. *Let $(f, (a_m))$ fulfil the weighted averaging condition with the weights a generating a measure. Then for any open measurable set $S \subset \mathbb{R}^d_+$*

$$\frac{1}{|S_L|_a} \sum_{m\in S_L} a_m \cdot f(m_1 x_1^0, m_2 x_2^0, \ldots, m_d x_d^0) \xrightarrow{L\to\infty} \int_{[0,1]^d} f(x)\,\mathrm{d}x\ .$$

Proof. We prove this in two steps. We call S_L the summation domain. First we show that the weighted averaging condition also holds for summation domains which are rectangles not aligned at the origin (i.e. we shift the Q_L out of the origin). Second, we cover S by a disjoint union of such rectangles and conclude the proof. Consider the scaled rectangle $R_L = \otimes_{i=1}^d \{\beta_i L, \ldots, \gamma_i L\} \subset \mathbb{N}^d$.

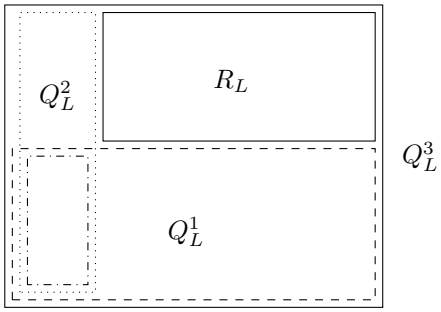

FIGURE 5. Construction of R_L from rectangles with one vertex in the origin: $R_L = Q_L^3 \setminus (Q_L^1 \cup Q_L^2)$

Then R_L can be constructed by making unions and subtractions of origin-aligned rectangles of the form Q_L as depicted in Figure 5. Thus

$$\frac{1}{|R_L|_a} \sum_{m\in R_L} a_m \cdot f(m_1 x_1^0, m_2 x_2^0, \ldots, m_d x_d^0) \xrightarrow{L\to\infty} \int_{[0,1]^d} f(x)\,\mathrm{d}x,$$

follows immediately.

For every approximation threshold $\delta > 0$ there are finite sets of squares $\{P_i\}_i$ and $\{O_i\}_i$ fulfilling

$$M_\delta = \bigcup_i P_i \subset S \subset \bigcup_i O_i = N_\delta.$$

with $\lambda(N_\delta \setminus S) \leq \lambda(N_\delta \setminus M_\delta) < \delta$. Write $(M_{\delta,L} = M_\delta \cdot L) \cap \mathbb{N}^d$, $P_{i,L} = (P_i \cdot L) \cap \mathbb{N}^d$ and $N_{\delta,L} = (N_\delta \cdot L) \cap \mathbb{N}^d$ analogously to S and S_L. We write $f(m \odot x^0) = f(m_1 x_1^0, m_2 x_2^0, \dots, m_d x_d^0)$ for brevity. Then we can derive the following error estimate

$$\begin{aligned}
\mathrm{Err} &= \left| \frac{1}{|N_{\delta,L}|_a} \sum_{m \in N_{\delta,L}} a_m f\left(m \odot x^0\right) - \frac{1}{|S_L|_a} \sum_{m \in S_L} a_m f\left(m \odot x^0\right) \right| \\
&= \frac{1}{|N_{\delta,L}|_a \cdot |S_L|_a} \left| |S_L|_a \sum_{m \in N_{\delta,L}} a_m f\left(m \odot x^0\right) - |N_{\delta,L}|_a \sum_{m \in S_L} a_m f\left(m \odot x^0\right) \right| \\
&= \frac{1}{|N_{\delta,L}|_a \cdot |S_L|_a} \left| (|N_{\delta,L}|_a - |S_L|_a) \sum_{m \in S_L} a_m f\left(m \odot x^0\right) + |S_L|_a \sum_{m \in N_{\delta,L} \setminus S_L} a_m f\left(m \odot x^0\right) \right| \\
&\leq \frac{1}{|N_{\delta,L}|_a \cdot |S_L|_a} \left| (|N_{\delta,L}|_a - |S_L|_a) \, \|f\|_\infty \sum_{m \in S_L} a_m \right| + \frac{1}{|N_{\delta,L}|_a \cdot |S_L|_a} \left| |S_L|_a \cdot \|f\|_\infty \sum_{m \in N_{\delta,L} \setminus S_L} a_m \right| \\
&= 2\|f\|_\infty \cdot \frac{||N_{\delta,L}|_a - |S_L|_a|}{|N_{\delta,L}|_a} = 2\|f\|_\infty \cdot \frac{|N_{\delta,L} \setminus S_L|_a}{|N_{\delta,L}|_a} \xrightarrow{L \to \infty} 2\|f\|_\infty \cdot \frac{\lambda_a(N_\delta \setminus S)}{\lambda_a(N_\delta)} \xrightarrow{\delta \to 0} 0,
\end{aligned}$$

where in the last step we use that the weight a generates a measure λ_a equivalent to the Lebesgue measure. Thus $\lambda_a(N_\delta) \to \lambda_a(S) > 0$ and $\lambda_a(N_\delta \setminus S) \to \lambda_a(\varnothing) = 0$.

Hence the approximation error has for all $\delta > 0$ a limit for $L \to \infty$ which is arbitrarily small for $\delta \to 0$, and it remains to check the limit on the cubical approximation N_δ instead of S, but this is straightforward:

$$\frac{1}{|N_{\delta,L}|} \sum_{m \in M_{\delta,L}} f(m \odot x^0) = \frac{1}{|N_{\delta,L}|} \sum_{\substack{P_{i,L} \\ \cup_i P_{i,L} = N_{\delta,L}}} |P_{i,L}| \cdot \frac{1}{|P_{i,L}|} \sum_{m \in P_{i,L}} f(m \odot x^0) \xrightarrow{L \to \infty} \int_{[0,1]^d} f(x) \, \mathrm{d}x,$$

according to the first step of this proof. □

3.3. **Weighted averages.** Here we present an elementary result showing that if the averages converge then the weighted averages do, too.

Lemma 10. *Given two sequences $\{b_k\}_k$ and $\{f_k\}_k$, such that $b_k \geq 0$ for all k, if*

$$F_N = \frac{1}{N} \sum_{k=1}^{N} f_k \xrightarrow{N \to \infty} 0,$$

and also $\frac{a_N \cdot N}{\sum_{k=1}^N a_k} \xrightarrow{N \to \infty} a$, for some $a \in \mathbb{R}$, with $a_k = \sum_{n=1}^k b_n$, and $\sum_{k=1}^N a_k \xrightarrow{N \to \infty} \infty$, then

$$\frac{\sum_{k=1}^N a_k \cdot f_k}{\sum_{k=1}^N a_k} \xrightarrow{N \to \infty} 0.$$

Proof. Consider first

$$\sum_{n=1}^{N} n \cdot b_n = \sum_{n=1}^{N} b_n \cdot N - \sum_{n=1}^{N-1} 1 \cdot \sum_{k=1}^{n} b_k = N \cdot a_N - \sum_{n=1}^{N-1} a_n,$$

which means that

$$\frac{\sum_{n=1}^{N} n \cdot b_n}{\sum_{n=1}^{N} a_n} \xrightarrow{N\to\infty} a - 1.$$

Now

$$\begin{aligned}
\frac{\sum_{k=1}^{N} a_k f_k}{\sum_{k=1}^{N} a_k} &= \frac{\sum_{k=1}^{N} \sum_{n=1}^{k} b_n \cdot f_k}{\sum_{k=1}^{N} a_k} \\
&= \frac{\sum_{n=1}^{N} b_n \cdot \sum_{k=n}^{N} f_k}{\sum_{k=1}^{N} a_k} \\
&= \frac{N}{\sum_{k=1}^{N} a_k} \sum_{n=1}^{N} \left[b_n \cdot F_N - b_n \cdot \frac{n}{N} \cdot F_n \right] \\
&= F_N \cdot \frac{N \cdot a_N}{\sum_{k=1}^{N} a_k} - \sum_{n=1}^{N} F_n \cdot \frac{n \cdot b_n}{\sum_{k=1}^{N} a_k}.
\end{aligned}$$

Note that $\sum_{n=1}^{N} F_n \cdot \frac{n \cdot b_n}{\sum_{k=1}^{N} a_k}$ is bounded by a constant C and there is N_1 such that $|F_N \cdot \frac{N \cdot a_N}{\sum_{k=1}^{N} a_k}| < \frac{\varepsilon}{3}$ for $n > N_1$. Also, there exists N_2, such that for $n > N_2$ we have

$$\left| \sum_{n=1}^{N_2} F_n \cdot \frac{n \cdot b_n}{\sum_{k=1}^{N} a_k} \right| \leq C \cdot \frac{\sum_{k=1}^{N_2} a_k}{\sum_{k=1}^{N} a_k} \leq \frac{\varepsilon}{3}.$$

Lastly we can choose N_3 such that for $N \geq N_3$

$$\left| \sum_{n=1}^{N_2} F_n \cdot \frac{n \cdot b_n}{\sum_{k=1}^{N} a_k} \right| < \frac{\varepsilon}{3}.$$

Then

$$\begin{aligned}
\left| \frac{\sum_{k=1}^{N} a_k f_k}{\sum_{k=1}^{N} a_k} \right| &\leq \left| F_N \cdot \frac{N \cdot a_N}{\sum_{k=1}^{N} a_k} \right| + \left| \sum_{n=1}^{N_2} F_n \cdot \frac{n \cdot b_n}{\sum_{k=1}^{N} a_k} \right| + \left| \sum_{n=N_2+1}^{N} F_n \cdot \frac{n \cdot b_n}{\sum_{k=1}^{N} a_k} \right| \\
&< \varepsilon
\end{aligned}$$

for $n > \max(N_1, N_2, N_3)$. □

The following corollary follows immediately by setting $f = g - C$.

Corollary 11. *Let the coefficients a_k be as in Lemma 10. If*

$$\frac{1}{N} \sum_{k=1}^{N} g_k \xrightarrow{N\to\infty} C,$$

then

$$\frac{\sum_{k=1}^{N} a_k \cdot g_k}{\sum_{k=1}^{N} a_k} \xrightarrow{N\to\infty} C.$$

3.4. **Asymptotic behaviour of the S_i.** Now we turn to the main technical tool to prove the main result.

Lemma 12. *For $x, t \in (0,1)$,*

$$\lim_{\varepsilon\to 0} \frac{1}{|R_\varepsilon|} \cdot S_1 = \frac{1}{4} \tag{5}$$

$$\lim_{\varepsilon\to 0} \varepsilon^2 \cdot \frac{S_3}{S_1} = \frac{1}{4} \tag{6}$$

$$\lim_{\varepsilon\to 0} \varepsilon \cdot \frac{S_2}{S_1} = 0. \tag{7}$$

Remark 13. *In the following proof we will show that the weighted averaging condition holds for $x, t \notin \mathbb{Q}$ by using Birkhoff's ergodic theorem 5. This leaves out the case when either x or t are in $\mathbb{Q}$. We have two ways of addressing this issue. We can compute explicitly the terms and obtain analytically the convergence required for the weighted average condition; these are straightforward but tedious computations, a sample of which is provided in the appendix, in Subsection A.*

At the same time we can observe that it is enough to have the limits almost everywhere in x, t, as we are integrating $W_t(x)$ and the Lebesgue integral ignores sets of null measure.

Proof of Lemma 12. As discussed above, we will consider only the case $x, t \notin \mathbb{Q}$.

We first prove (5). We can use Birkhoff's ergodic theorem. Define $T_x(z) = z + x$: this is a measure-preserving and uniquely ergodic transformation (since $x \notin \mathbb{Q}$). Then

$$\frac{1}{N}\sum_{k=0}^{N-1} \cos^2(\pi k x) = \frac{1}{N}\sum_{k=0}^{N-1} \cos^2\left(\pi T_x^k(0)\right) \xrightarrow{N\to\infty} \int_0^1 \cos^2(\pi x)\,\mathrm{d}x = \frac{1}{2}.$$

All the coefficients a_m are 1 in this case and the function is multiplicative. Then the result follows immediately from Lemma 9 and the fact that

$$\int_{[0,1]^2} \cos^2(\pi x_1)\cos^2(\pi x_2)\,\mathrm{d}(x_1, x_2) = \frac{1}{4}.$$

We prove now (6). For $x, t \notin \mathbb{Q}$ we know from (5) that the denominator $S_1 \sim \frac{|R_\varepsilon|}{4}$ as $\varepsilon \to 0$ for $x \neq 0, 1$. Hence the term in question has the same asymptotic behaviour as

$$\varepsilon^2 \frac{S_3}{S_1} \sim 4\pi^2 \frac{\varepsilon^2}{|R_\varepsilon|} \cdot \sum_{k,l\in R_\varepsilon} k^2 \sin^2(k\pi x)\cos^2(l\pi t). \tag{8}$$

We define $a = (a_{k,l})_{k,l}$ with $a_{k,l} = k^2$, where we already saw in our example that his generates a measure with Lebesgue density such that

$$\lim_{\varepsilon\to 0} \varepsilon^2 \cdot \frac{|R_\varepsilon|_a}{|R_\varepsilon|} = \lim_{\varepsilon\to 0} \varepsilon^2 \cdot \frac{1}{|R_\varepsilon|} \sum_{k,l\in R_\varepsilon} k^2 = \frac{\lambda_a(R)}{\lambda(R)}, \tag{9}$$

where the rescaled domain is

$$R = \{(\eta, \xi) \in \mathbb{R}^2 |\ \alpha_\ominus < \sqrt{\xi^2 + \eta^2} < \alpha_\oplus\},$$

which gives

$$R_\varepsilon = \varepsilon^{-1} R \cap \mathbb{N}^2.$$

As $\mathrm{d}\lambda_a = \eta^2\,\mathrm{d}(\eta,\xi)$ we obtain by elementary calculations using polar coordinates

$$\begin{aligned}\frac{\lambda_a(R)}{\lambda(R)} &= \frac{4}{\pi(\alpha_\oplus^2-\alpha_\ominus^2)}\int_R \eta^2\,\mathrm{d}(\eta,\xi)\\ &= \frac{4}{\pi(\alpha_\oplus^2-\alpha_\ominus^2)}\int_0^{\pi/2}\int_{\alpha_\ominus}^{\alpha_\oplus} r^3\cos(\varphi)^2\,\mathrm{d}r\,\mathrm{d}\varphi = \frac{1}{\alpha_\oplus^2-\alpha_\ominus^2}\int_{\alpha_\ominus}^{\alpha_\oplus} r^3\,\mathrm{d}r\\ &= \frac{1}{4}\frac{\alpha_\oplus^4-\alpha_\ominus^4}{\alpha_\oplus^2-\alpha_\ominus^2} = \frac{1}{4}(\alpha_\oplus^2+\alpha_\ominus^2) = \frac{1}{4\pi^2}\,.\end{aligned}$$

Combining (8) and (9), it remains to show that we can apply the averaged Birkhoff ergodic theorem to the sum. We already saw that it is sufficient to check this on large rectangles containing the origin. We define Q_L as in the weighted averaging condition for $\alpha \in (0,\infty)^2$ so that

$$Q_L = [1,\alpha_1 L]\times[1,\alpha_2 L]\cap\mathbb{N}^2 = I_L^{(1)}\times I_L^{(2)} \quad \text{with} \quad I_L^{(j)} = [1,\alpha_j L]\cap\mathbb{N}\,.$$

Because of the rectangular shape we can split the sum

$$\begin{aligned}\frac{1}{|Q_L|_a}\cdot\sum_{(k,l)\in Q_L} k^2\sin^2(k\pi x)\cos^2(l\pi t) &= \frac{1}{\sum_{k\in I_L^{(1)}}k^2}\cdot\sum_{k\in I_L^{(1)}}k^2\sin^2(k\pi x)\cdot\frac{1}{\sum_{l\in I_L^{(2)}}1}\sum_{l\in I_L^{(2)}}\cos^2(l\pi t)\\ &\sim \frac{1}{|I_L^{(1)}|}\cdot\sum_{k\in I_L^{(1)}}\sin^2(k\pi x)\cdot\frac{1}{|I_L^{(2)}|}\sum_{l\in I_L^{(2)}}\cos^2(l\pi t)\\ &\xrightarrow{L\to\infty}\frac{1}{4}\,,\end{aligned}$$

by the standard one-dimensional ergodic theorem, where we used Corollary 11 to remove the weights. We can now use Lemma 9 to extend this to the ring and obtain

$$\varepsilon^2\cdot\frac{S_3}{S_1}\sim 4\pi^2\varepsilon^2\cdot\frac{|R_\varepsilon|_a}{|R_\varepsilon|}\cdot\frac{1}{|R_\varepsilon|_a}\cdot\sum_{k,l\in R_\varepsilon}k^2\sin^2(k\pi x)\cos^2(l\pi t)\xrightarrow{\varepsilon\to 0}\frac{1}{4},$$

where we evaluated the value of the limit in (9).

Finally, we prove (7). As it was the case in (6), we can calculate the sum of the coefficients, factor them out and see that the orders of magnitude of ε cancel out. Then everything is reduced to the integral

$$\int_{[0,1]^2}\cos(\pi x_1)\sin(\pi x_1)\cos^2(\pi x_2)\,\mathrm{d}(x_1,x_2) = 0. \qquad \square$$

3.5. **Proof of main result.** We have now all the ingredients to complete the proof of Theorem 2.

Proof of Theorem 2. From Lemma 12 we know that

$$W_t(x) = \frac{S_3}{S_1} - \left(\frac{S_2}{S_1}\right)^2 \sim \frac{1}{4\varepsilon^2} \qquad \text{as } \varepsilon\to 0.$$

By Theorem 1, the number of expected zeros on the horizontal line L_t of length 1 is, for a given ε,

$$N = \frac{1}{\pi}\int_0^1\sqrt{\frac{1}{4\varepsilon^2}}\,\mathrm{d}x = \frac{1}{2\pi\cdot\varepsilon}.$$

This is the same as saying that the average pattern size is $\frac{1}{N} = 2\pi\varepsilon$. $\square$

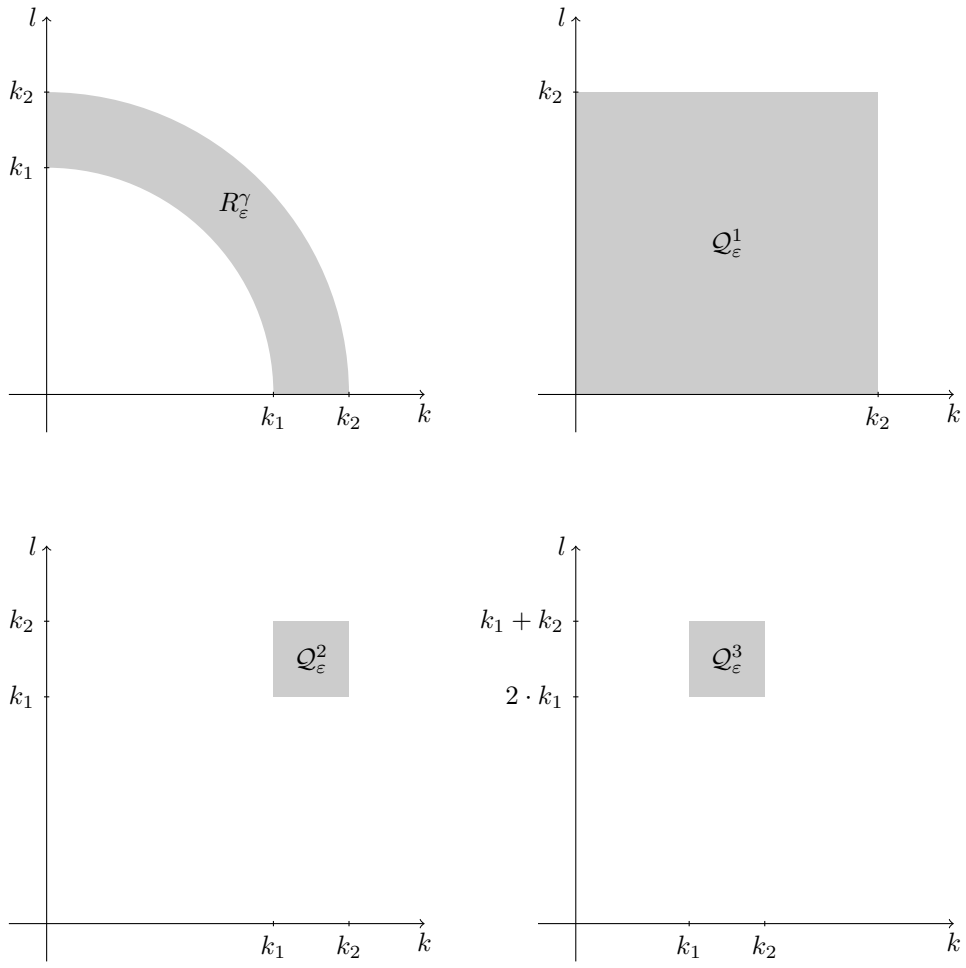

FIGURE 6. The ring R^γ and the alternative mode domains $\mathcal{Q}^i$, $i = 1, 2, 3$.

4. General Fourier domains

We can consider domains in Fourier space that are different from the ring. The main difference is that we get a different constant, which depends on the shape of the Fourier-domain. Also the constant might be different along different directions if we lose the symmetry in k and l in the Fourier space, but we will discuss that later in Section 6. On the other hand for horizontal lines we can give an explicit constant, in terms of the measure λ_a, and for vertical lines we can argue by symmetry. Let us discuss a few explicit examples.

Consider the following mode domains where we define as before for some $\gamma \in (0, 1)$

$$k_1 = \frac{\alpha_\ominus}{\varepsilon} = \sqrt{\frac{1-\sqrt{1-\gamma}}{2\pi^2\varepsilon^2}} \quad \text{and} \quad k_2 = \frac{\alpha_\oplus}{\varepsilon} = \sqrt{\frac{1+\sqrt{1-\gamma}}{2\pi^2\varepsilon^2}}$$

$$
\begin{aligned}
R_\varepsilon^\gamma &= \{(k,l) \in \mathbb{N}^2 |\ k_1 < \sqrt{k^2+l^2} < k_2\},\\
\mathcal{Q}_\varepsilon^1 &= \{(k,l) \in \mathbb{N}^2 |\ 0 < k,l < k_2\},\\
\mathcal{Q}_\varepsilon^2 &= \{(k,l) \in \mathbb{N}^2 |\ k_1 < k,l < k_2\},\\
\mathcal{Q}_\varepsilon^3 &= \{(k,l) \in \mathbb{N}^2 |\ k_1 < k < k_2,\ 2k_1 < l < k_1+k_2\}.
\end{aligned}
$$

Note that R_ε^γ is the same quarter-ring-shaped domain as before and the others are certain rectangles, all of them represented in Figure 6. For our main result, we will also use the scaled ε-independent versions

$$R^\gamma = \{(\eta,\xi) \in \mathbb{R}^2 |\ \alpha_\ominus < \sqrt{\xi^2+\eta^2} < \alpha_\oplus\}$$

$$\mathcal{Q}^1 = (0,\alpha_\oplus)^2, \quad \mathcal{Q}^2 = (\alpha_\ominus,\alpha_\oplus)^2, \quad \mathcal{Q}^3 = (\alpha_\ominus,\alpha_\oplus)\times(2\alpha_\ominus,\alpha_\ominus+\alpha_\oplus),$$

so that

$$R_\varepsilon^\gamma = \varepsilon^{-1}R^\gamma \cap \mathbb{N}^2 \quad \text{and} \quad \mathcal{Q}_\varepsilon^i = \varepsilon^{-1}\mathcal{Q}^i \cap \mathbb{N}^2 \text{ for } i = 1,2,3\ .$$

We provide numerical simulations on how the patterns look like on such domains in Figure 7. They look quite different, although as we will see in the following Lemma 14, the main result about the asymptotic distribution of zeros is the same in all four cases, only the constants change.

Lemma 14. *Let $D_\varepsilon = \varepsilon^{-1}D \cap \mathbb{N}^2$ be a scaled domain in Fourier space (for example R_ε^γ or $\mathcal{Q}_\varepsilon^i$ for $i = 1,2,3$). Then the asymptotic (for $\varepsilon \to 0$) density of zeros δ is on horizontal lines through the pattern*

$$\delta(x) \sim \frac{1}{2\pi\varepsilon}\cdot\sqrt{\frac{\lambda_{(k^2,1)}(D)}{\lambda(D)}},$$

while on vertical lines it is

$$\delta(x) \sim \frac{1}{2\pi\varepsilon}\cdot\sqrt{\frac{\lambda_{(1,l^2)}(D)}{\lambda(D)}}.$$

Proof. This is a proof analogous to the one of Lemma 12. We obtain the following asymptotic equivalences

$$\delta(x)^2 \sim \frac{S_3}{S_1} \sim \frac{1}{4}\cdot\frac{|D_\varepsilon|_{(k^2,1)}}{|D_\varepsilon|} \sim \frac{1}{4\varepsilon^2}\cdot\frac{\lambda_{(k^2,1)}(D)}{\lambda(D)}.$$

The statement on vertical lines simply follows by symmetry. □

The correction factors $\lambda_a(D)/\lambda(D)$ for the weights $a_{k,l} = k^2$ and the pattern sizes in the following domains are

Domain	Correction coeff.	Avg. number of zeros	Avg. pattern size
R_ε^γ	1	$\frac{1}{2\pi\varepsilon}$	$2\pi\varepsilon$
$\mathcal{Q}_\varepsilon^1$	$\frac{2}{3}(1+\sqrt{1-\gamma})$	$\frac{\sqrt{\frac{2}{3}(1+\sqrt{1-\gamma})}}{2\pi\varepsilon}$	$\frac{2\pi\varepsilon}{\sqrt{\frac{2}{3}(1+\sqrt{1-\gamma})}}$
$\mathcal{Q}_\varepsilon^2$	$\frac{2}{3}(2+\sqrt{\gamma})$	$\frac{\sqrt{\frac{2}{3}(2+\sqrt{\gamma})}}{2\pi\varepsilon}$	$\frac{2\pi\varepsilon}{\sqrt{\frac{2}{3}(2+\sqrt{\gamma})}}$

These are due to symmetry the same results for horizontal or vertical lines, while for the non-symmetric $\mathcal{Q}^3$ we have

$\mathcal{Q}_\varepsilon^3$	Correction coeff.	Avg. number of zeros	Avg. pattern size
horizontal	$\frac{2}{3}(2+\sqrt{\gamma})$	$\frac{\sqrt{\frac{2}{3}(2+\sqrt{\gamma})}}{2\pi\varepsilon}$	$\frac{2\pi\varepsilon}{\sqrt{\frac{2}{3}(2+\sqrt{\gamma})}}$
vertical	$\frac{2}{3}(8-6\sqrt{1-\gamma}+4\sqrt{\gamma})$	$\frac{\sqrt{\frac{2}{3}(8-6\sqrt{1-\gamma}+4\sqrt{\gamma})}}{2\pi\varepsilon}$	$\frac{2\pi\varepsilon}{\sqrt{\frac{2}{3}(8-6\sqrt{1-\gamma}+4\sqrt{\gamma})}}$.

In Figure 7 the simulations are run with $\gamma = 0.7$ and 10^{-2}. In those cases we have the following rounded off asymptotic values for the number of zeros on a line:

Domain	Correction coeff.	Avg. number of zeros	Avg. pattern size
$R_{0.01}^{0.7}$	1	15.915 ($\times 1$)	0.062832
$\mathcal{Q}_{0.01}^1$	1.032	16.167 ($\times 1.016$)	0.061856
$\mathcal{Q}_{0.01}^2$	1.891	21.887 ($\times 1.375$)	0.045690
$\mathcal{Q}_{0.01}^3$ (hor.)	1.891	21.887 ($\times 1.375$)	0.045690
$\mathcal{Q}_{0.01}^3$ (ver.)	5.374	36.894 ($\times 2.318$)	0.027105.

If we sample random vertical lines in the numerical simulations represented in Figure 7, we get the following number of zeros, which are in good agreement with the predicted asymptotic results.

Domain	Avg. number of zeros (sampled)
$R_{0.01}^{0.7}$	16.413
$\mathcal{Q}_{0.01}^1$	16.984
$\mathcal{Q}_{0.01}^2$	21.931
$\mathcal{Q}_{0.01}^3$ (ver.)	37.315.

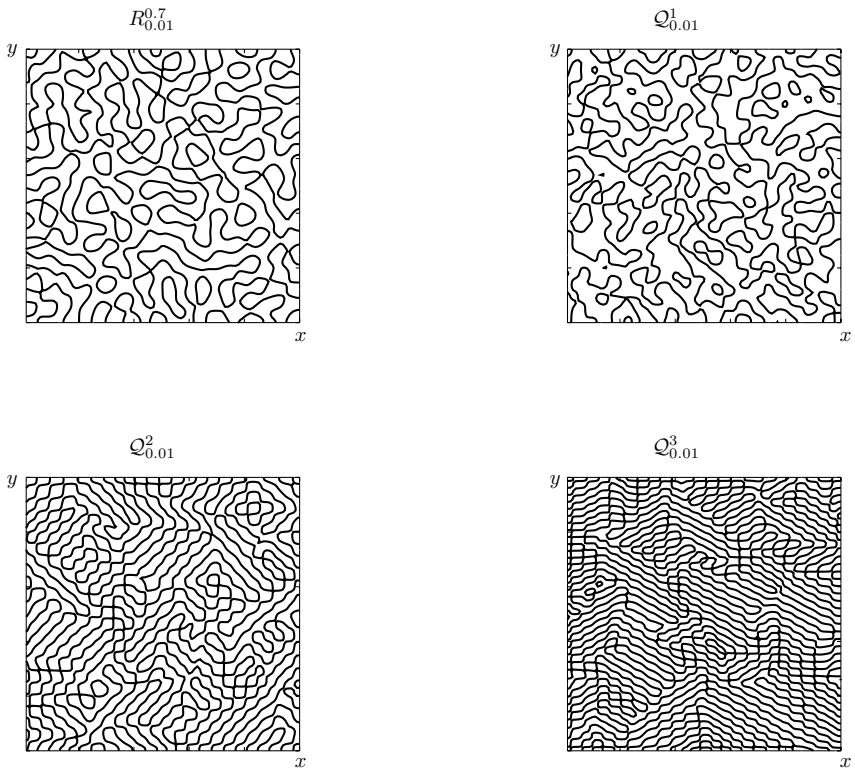

FIGURE 7. Patterns generated by the Fourier domains presented in Figure 6

5. Numerical Simulations

In Figure 8 we plot the (rescaled) density of zeros $\varepsilon\delta(x) = \frac{\varepsilon}{\pi}\sqrt{W_t(x)}$ for various values of ε on the domain $R^{0.8}$. We scale by ε so that the convergence to $1/2\pi$ is easily seen. We can observe that the density in fact converges pointwise (apart from $x = 0, 1$). It even seems that the convergence is uniform away from an arbitrarily small boundary layer.

It is interesting to fix a point $x_0 \in (0, 1)$ and to track the value of $\varepsilon\delta(x_0)$ for $\varepsilon \to 0$. This is done in Figure 9.

Once again we can read off the convergence to $1/2\pi$ but we can also quantify the convergence's disturbance by the "travelling wave" which goes to the borders of the interval: even if we choose a point which is very close to 0 (the critical points), for example $x_0 = 10^{-2}$, we see that the magnitude of the density grows very quickly at first until it hits the limit value and then exhibits a damped oscillation around that asymptotic growth rate. When compared to Figure 8, we can imagine those travelling waves approaching and going through such a value x_0 until after some threshold ε, the oscillation is negligible.

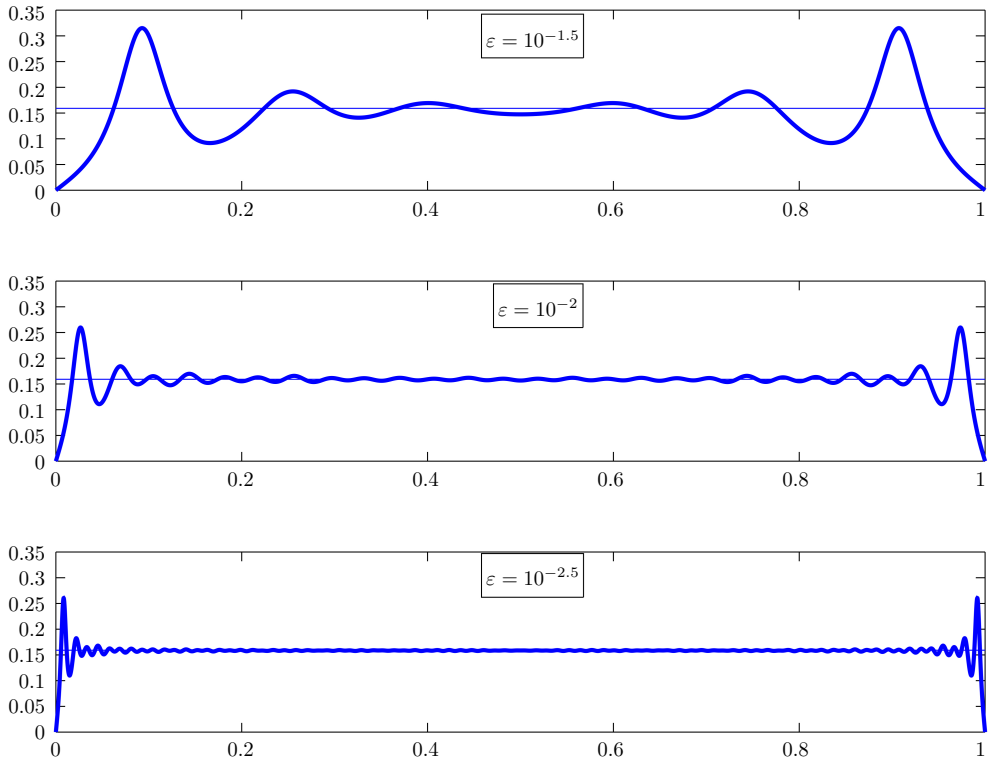

FIGURE 8. Zeros density for $t = 0.5$ and $\gamma = 0.8$ (multiplied by ε) for some values of ε on the ring-shaped domain. These pictures are a graphical representation of the pointwise limit $\varepsilon\delta(x) \to \frac{1}{2\pi}$ proven in Theorem 2.

6. Sloped lines

As we have already mentioned, the result given in Theorem 2 is proven only for horizontal lines and by symmetry for vertical lines. We claim that the result is far more general. In order to do so, we consider any sloped line through the origin. For the ring R^γ we will see that we obtain the same asymptotic behaviour.

To fix the setting we assume $y = \mu x$, with $\mu \in (0, 1]$. This last assumption is just for simplicity of presentation, as we can use the reflection at the diagonal to get the analogous result for the remaining half square.

Note that considering lines through the origin is not restrictive, we do this only for simplicity of presentation. The more general case $y = \mu x + \tau$ behaves in the same way, using the trigonometric formulas for the cosine of a sum, which just adds to the number of the terms involved.

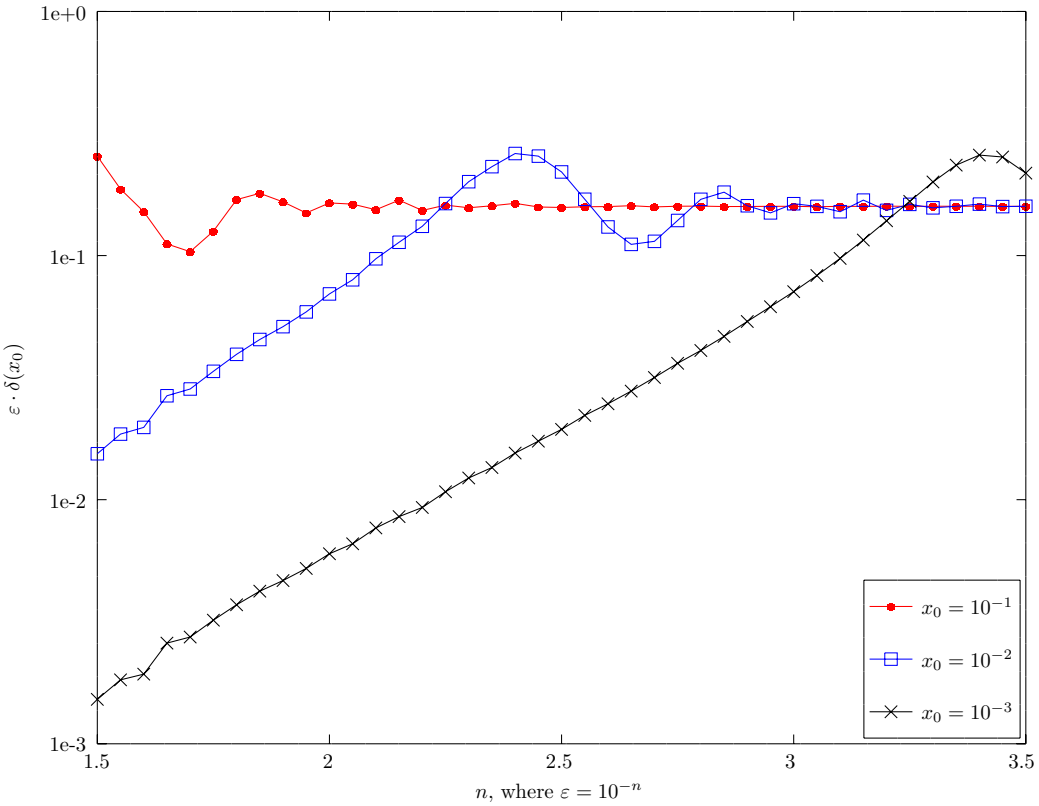

FIGURE 9. Values for $\varepsilon\delta(x_0)$ for various values of x_0. The parameter ε is on the abscissa and the scaled value of the density is on the ordinate.

The important thing in that situation is to consider only the intersection $(x, \mu x + \tau) \cap [0,1]^2$, so we have to pay attention to the x's that are in our domain, and to the corresponding length of the segment we need for the renormalisation.

For $y = \mu x$, we have, instead of $w_t(x)$, the following vector of functions:

$$w_\mu(x) = \left(\cos(k\pi x)\cos(l\pi\mu x) / \left(\sum_{m,n} \cos^2(m\pi x)\cos^2(n\pi\mu x) \right)^{1/2} \right)_{k,l}$$

and also

$$W_\mu(x) = \frac{\sum_{k,l}\left[-S_1(k\pi\sin(k\pi x)\cos(l\pi\mu x) + l\pi\mu\sin(l\pi\mu x)\cos(k\pi x)) + \cos(k\pi x)\cos(l\pi\mu x)\tilde{S}_2\right]^2}{(S_1)^3}$$
$$= \frac{\sum_{k,l}(k\pi\sin(k\pi x)\cos(l\pi\mu x) + l\pi\mu\sin(l\pi\mu x)\cos(k\pi x))^2}{S_1} - \left(\frac{\tilde{S}_2}{S_1}\right)^2$$
$$= \frac{\tilde{S}_3}{S_1} - \left(\frac{\tilde{S}_2}{S_1}\right)^2,$$

where S_1 is as in the horizontal case with $t := \mu x$ and

$$\tilde{S}_2 = \sum_{k,l}\cos(k\pi x)\cos(l\pi t)(k\pi\sin(k\pi x)\cos(l\pi t) + l\pi\mu\sin(l\pi t)\cos(k\pi x))$$
$$\tilde{S}_3 = \sum_{k,l}(k\pi\sin(k\pi x)\cos(l\pi t) + l\pi\mu\sin(l\pi t)\cos(k\pi x))^2,$$

which are the generalisations of the S_2 and S_3 encountered before. To prove that things work the same way in this case, we have to prove first the following:

$$\lim_{\varepsilon\to 0}\varepsilon^2\left(\frac{\tilde{S}_2}{S_1}\right)^2 = 0. \tag{10}$$

This can be shown with arguments analogous to those for horizontal lines. The main new tool we need is that the averaging works for weights $(k,1)$, $(1,l)$, and (k,l). Then we need to notice that any term with a sin-function averages in the limit to 0 in the Birkhoff ergodic theorem. This implies (10).

Secondly, with the same argument, we see the following asymptotic equivalence

$$\varepsilon^2\frac{\tilde{S}_3}{S_1} \sim \varepsilon^2\frac{1}{S_1}\Big(\sum_{k,l}k^2\pi^2\sin(k\pi x)^2\cos(l\pi\mu x)^2 + \mu^2\sum_{k,l}l^2\pi^2\sin(l\pi\mu x)^2\cos(k\pi x)^2\Big)$$

This implies the following Theorem:

Theorem 15. *For sloped lines $y = \mu x$ with $\mu \in [0.1]$ and general Fourier-domains D we have that*

$$\delta(x)^2 \sim \frac{1}{4\varepsilon^2}\cdot\frac{1}{\lambda(D)}\Big(\lambda_{(k^2,1)}(D) + \mu^2\lambda_{(1,l^2)}(D)\Big).$$

If the domain D is symmetric with respect to the reflection along the diagonal like the ring R^γ or the squares $\mathcal{Q}_1$ and $\mathcal{Q}_2$. Then $\delta(x)^2$ is compared to a horizontal line just modified by a factor $(1+\mu^2)$. But this just compensates the length of the segment, which is not 1 as before but $\sqrt{1+\mu^2}$. Now the two factors cancel and the average pattern size is for every sloped line the same as for the horizontal line.

Thus we obtain in the symmetric examples like R^γ, $\mathcal{Q}_1$, and $\mathcal{Q}_2$ that for any sloped line the average pattern size is for every sloped line the same and of order ε.

Appendix A. The rational case

In the proof of Lemma 12 we only considered irrational values of x and t. This is sufficient because we are interested in the density on a set of Lebesgue-measure 1 because we integrate it anyway. But as an additional consideration, for rational values, the periodicity of trigonometric functions yields a non-ergodic averaging result of the same type as on the irrational numbers.

We restrict ourselves to a particularly easy case but the actual proof is a straightforward generalization.

Let $x = \frac{1}{n}$ and $N = l \cdot n$ for $l, n \in \mathbb{N}$ without loss of generalization and consider

$$\begin{aligned}\frac{1}{N}\sum_{k=1}^{N}\cos^2(k\pi x) &= \frac{1}{2N}\sum_{k=1}^{N}\cos(2\pi k\frac{1}{n}) \\ &= \frac{1}{2} + \frac{1}{2}\cdot\left(\frac{1}{2}\frac{\sin(\frac{2\pi N+\pi}{n})-1}{\sin(\frac{\pi}{n})}\right) \\ &= \frac{1}{2} - \frac{1}{4N} \xrightarrow{N\to\infty} \frac{1}{2}.\end{aligned}$$

This corresponds nicely to the ergodic result

$$\lim_{N\to\infty}\frac{1}{N}\sum_{k=1}^{N}\cos^2(k\pi x) = \frac{1}{2}$$

for irrational x. In this way, we can for example prove

$$\frac{1}{|R_\varepsilon|}S_1 = \frac{1}{|R_\varepsilon|}\sum_{k,l\in R_\varepsilon}\cos^2(k\pi x)\cos^2(l\pi t) \xrightarrow{N\to\infty} \frac{1}{4}.$$

Acknowledgments

The authors want to thank Thomas Wanner for pointing out the result by Edelman and Kostlan. Moreover, Blömker & Wacker would like to thank Evelyn Sander and Thomas Wanner for their hospitality.

References

[1] R. J. Adler and J. E. Taylor. *Random fields and geometry.* New York, NY: Springer, 2007.
[2] R. J. Adler and J. E. Taylor. *Topological complexity of smooth random functions. École d'Été de Probabilités de Saint-Flour XXXIX-2009.* Berlin: Springer, 2011.
[3] J. Baxter and J. Olsen. Weighted and subsequential ergodic theorems. *Can. J. Math., 3_5*, pages 145–166, 1983.
[4] A. Bellow and V. Losert. The weighted pointwise ergodic theorem and the individual ergodic theorem along subsequences. *Transactions of the American Mathematical Society*, 288(1):307–345, 1985.
[5] D. Blömker and S. Maier-Paape. Pattern formation below criticality forced by noise. *Zeitschrift für angewandte Mathematik und Physik (ZAMP)*, 54(1):1–25, 2003.
[6] D. Blömker, S. Maier-Paape, and T. Wanner. Spinodal decomposition for the Cahn-Hilliard-Cook equation. *Communications in Mathematical Physics*, 223:553–582, 2001.
[7] D. Blömker, S. Maier-Paape, and T. Wanner. Phase separation in stochastic Cahn-Hilliard models. In A. Miranville, editor, *Mathematical Methods and Models in Phase Transitions*, pages 1–41. Nova Science Publishers, New York, 2005.
[8] D. Blömker, S. Maier-Paape, and T. Wanner. Second phase spinodal decomposition for the Cahn-Hilliard-Cook equation. *Transactions of the American Mathematical Society*, 360(1):449–489, 2008.
[9] D. Blömker and M. Romito. Stochastic PDEs and lack of regularity. (A surface growth equation with noise: existence, uniqueness, and blow-up). *Jahresberichte der DMV*, 2015. to appear.

[10] J. W. Cahn. Free energy of a nonuniform system, II. Thermodynamic basis. *Journal of Chemical Physics*, 30:1121–1124, 1959.
[11] J. W. Cahn and J. E. Hilliard. Free energy of a nonuniform system, I. Interfacial free energy. *Journal of Chemical Physics*, 28:258–267, 1958.
[12] H. Cook. Brownian Motion in Spinodal Decomposition. *Acta metallurgica*, 18:297–306, 1970.
[13] I. P. Cornfeld, S. V. Fomin, and Y. G. Sinai. *Ergodic theory*, volume 245 of *Grundlehren der mathematischen Wissenschaften*. Springer, 1982.
[14] M. C. Cross and P. C. Hohenberg. Pattern formation outside of equilibrium. *Reviews of modern physics*, 65(3):851, 1993.
[15] G. Da Prato and J. Zabczyk. *Stochastic equations in infinite dimensions*, volume 152 of *Encyclopedia of Mathematics and its Applications*. Cambridge University Press, 2 edition, 2014.
[16] S. Day, W. Kalies, K. Mischaikow, and T. Wanner. Probabilistic and numerical validation of homology computations for nodal domains. *Electronic Research Announcements of the American Mathematical Society*, 13(7):60–73, 2007.
[17] S. Day, W. Kalies, and T. Wanner. Verified homology computations for nodal domains. *Multiscale Modeling & Simulation*, 7(4):1695–1726, 2009.
[18] M. Dennis. Nodal densities of planar gaussian random waves. *The European Physical Journal Special Topics*, 145(1):191–210, 2007.
[19] A. Edelman and E. Kostlan. How many zeros of a random polynomial are real? *Bulletin of the American Mathematical Society*, 32(1):1–37, 1995.
[20] M. Gameiro, K. Mischaikow, and T. Wanner. Evolution of pattern complexity in the Cahn–Hilliard theory of phase separation. *Acta Materialia*, 53(3):693–704, 2005.
[21] A. Gorodnik and A. Nevo. *The Ergodic Theory of Lattice Subgroups*. Princeton University Press, 2009.
[22] A. Gorodnik and A. Nevo. Quantitative ergodic theorems and their number-theoretic applications. *Bull. Am. Math. Soc., New Ser.*, 52(1):65–113, 2015.
[23] Y. Guo and H. J. Hwang. Pattern formation. II: The Turing instability. *Proc. Am. Math. Soc.*, 135(9):2855–2866, 2007.
[24] D. L. Hanson and G. Pledger. On the mean ergodic theorem for weighted averages. *Zeitschrift für Wahrscheinlichkeitstheorie und Verwandte Gebiete*, 13(2):141–149, 1969.
[25] R. Hoppe and E. Nash. A combined spectral element/finite element approach to the numerical solution of a nonlinear evolution equation describing amorphous surface growth of thin films. *J. Numer. Math.*, 100(2):127–136, 2002.
[26] M. S. Longuet-Higgins. The statistical analysis of a random, moving surface. *Philosophical Transactions of the Royal Society of London A: Mathematical, Physical and Engineering Sciences*, 249(966):321–387, 1957.
[27] M. S. Longuet-Higgins. Statistical properties of an isotropic random surface. *Philosophical Transactions of the Royal Society of London A: Mathematical, Physical and Engineering Sciences*, 250(975):157–174, 1957.
[28] S. Maier-Paape and T. Wanner. Spinodal Decomposition for the Cahn–Hilliard Equation in Higher Dimensions. Part I: Probability and Wavelength Estimate. *Communications in Mathematical Physics*, 195(2):435–464, 1998.
[29] S. Maier-Paape and T. Wanner. Spinodal decomposition for the Cahn-Hilliard equation in higher dimensions, II: Nonlinear dynamics. *Arch. Ration. Mech. Anal.*, 151:187–219, 2000.
[30] J. Muñoz-García, R. Gago, L. Vázquez, J. A. Sánchez-García, and R. Cuerno. Observation and modeling of interrupted pattern coarsening: Surface nanostructuring by ion erosion. *Phys. Rev. Lett*, 104:026101, 2010.
[31] J. D. Murray. *Mathematical Biology II Spatial Models and Biomedical Applications*, volume 18 of *Interdisciplinary Applied Mathematics*. Springer, 2003.
[32] M. Raible, S. Linz, and P. Hänggi. Amorphous thin film growth: Effects of density inhomogeneities. *Phys. Rev. E*, 64:031506, 2001.
[33] S. O. Rice. Statistical properties of a sine wave plus random noise. *Bell System Technical Journal*, 27(1):109–157, 1948.
[34] E. Sander and R. Tatum. Pattern formation in a mixed local and nonlocal reaction-diffusion system. *Electron. J. Differ. Equ.*, 2012:30, 2012.
[35] E. Sander and T. Wanner. Unexpectedly linear behavior for the Cahn-Hilliard equation. *SIAM Journal on Applied Mathematics*, 60:2182–2202, 2000.
[36] E. Sander and T. Wanner. Pattern formation in a nonlinear model for animal coats. *J. Differ. Equations*, 191(1):143–174, 2003.

[37] E. Siero, A. Doelman, M. B. Eppinga, J. D. M. Rademacher, M. Rietkerk, and K. Siteur. Striped pattern selection by advective reaction-diffusion systems: Resilience of banded vegetation on slopes. *Chaos: An Interdisciplinary Journal of Nonlinear Science*, 25:036411, 2015.
[38] K. Siteur, E. Siero, M. Eppinga, J. D. M. Rademacher, A. Doelman, and M. Rietkerk. Beyond Turing: The response of patterned ecosystems to environmental change. *Ecol. Complexity*, 20:81–96, 2014.
[39] M. Sodin. Lectures on random nodal portraits.

L. A. Bianchi, Institut für Mathematik, Universität Augsburg, D-86135 Augsburg, Germany
E-mail address: luigi.bianchi@math.uni-augsburg.de
URL: http://www.math.uni-augsburg.de/prof/ana/arbeitsgruppe/bianchi/

D. Blömker, Institut für Mathematik, Universität Augsburg, D-86135 Augsburg, Germany
E-mail address: dirk.bloemker@math.uni-augsburg.de
URL: http://www.math.uni-augsburg.de/prof/ana/arbeitsgruppe/bloemker/

P. Wacker, Institut für Mathematik, Universität Augsburg, D-86135 Augsburg, Germany
E-mail address: dueren@math.uni-augsburg.de
URL: http://www.math.uni-augsburg.de/prof/ana/arbeitsgruppe/dueren/